BEACH INUNDATION PREDICTION DURING STORMS USING DIREFERENTS WAVE HEIGHTS AS INPUTS

Amanda Sancho-García[1], Jorge Guillén[1], Gonzalo Simarro[1], Raúl Medina[2] and Verónica Cánovas[2].

Beach inundation prediction is evaluated at an artificial, tideless embayed beach located in the city of Barcelona (NW Mediterranean, Spain). To this end, inundation measurements using video observations are compared with estimations including the tidal variations and the wave runup formulation of Stockdon et al. (2006), introducing deep water, local wave measurements and local wave computations as inputs. As the observations consider the mean runup and the estimations use the 2% runup exceedance ($R_{2\%}$), the inundation is overestimated if any of the wave heights in the formulation are used. Nonetheless, results are improved if a local wave height at 10 m depth is used, in particular for waves approaching the shore obliquely. Finally, it is stated that the differences between the observations and the estimations vary along the beach, being higher in the curved zone of the embayment.

Keywords: wave runup, embayed beaches, video monitoring.

INTRODUCTION

Coastal regions are frequently subject to inundation produced by storms. Storm-induced inundation is due to the sum of astronomical tide, surge level and wave runup. The surge levels are dependent on changes in the atmospheric pressure (e.g., low pressure systems) (Ciavola et al., 2011) and are largely affected by the bathymetric characteristics of the continental shelf (width and depth) (del Rio et al., 2012). In the tideless Mediterranean sea, surge levels as a whole are likely to be much lower because of the much greater water depth (Wolf, 2009), so wave runup may be the main process controlling beach inundation during storms (Bosom and Jimenez, 2011).

Wave runup is defined as the time-varying location of the waterline about still water level. It can be decomposed into *setup*, a steady elevation of mean water level, and *swash*, fluctuations about the setup level (Guza and Thornton, 1982). Most runup prediction formulations include a deep water wave height, H_{s0}, and have been developed for natural sandy, macrotidal and open oceanic beaches. The application of these approaches to beaches protected by coastal structures, where wave transformation processes (*e.g.* diffraction) can be relevant, remains unclear. So, the main goal of this study is using video images to evaluate whether wave transformation processes influence considerably the prediction capability of Stockdon et al. (2006) formulation for inundation at Somorrostro beach (Barcelona, Spain). It is considered three different characterizations of the wave height: H_{s0} (measured at deep water), H_{s1} (measured at 10 m depth) and H_{s2} (computed at 10m depth from deep water conditions using the SMC model by Gonzalez et al. (2007)).

Study area

Somorrostro beach is located in the city of Barcelona, on the southern coast of Catalonia, Spain, in the western Mediterranean Sea (Fig. 1). Barcelona has a coastline 13 km long, containing the city harbor in the southernmost part, three marinas and 3 km of beaches. Barcelona's beaches are artificial and were created as a part of the urban renewal that took place in the zone for the 1992 Olympic Games. This study focuses on Somorrostro beach, a non-barred beach bounded to the north by the Olympic Marina and to the south by a double dike. The beach is 400 m long and is oriented N32E. The tidal range is less than 20 cm and waves are the main stirring mechanism controlling coastal evolution (Ojeda and Guillén, 2008). The beach has a steep slope (β_f): on average $\beta_f = 0.080$, increasing slightly from south to north.

[1] Instituto de Ciencias del Mar (ICM-CSIC), Passeig Maritim de la Barceloneta 37-49, 08003 Barcelona, Spain.
[2] Environmental Hydraulics Institute "IH Cantabria", Universidad de Cantabria, c./ Isabel Torres nº15, PCTCAN,39011,Santander, Cantabria, Spain.

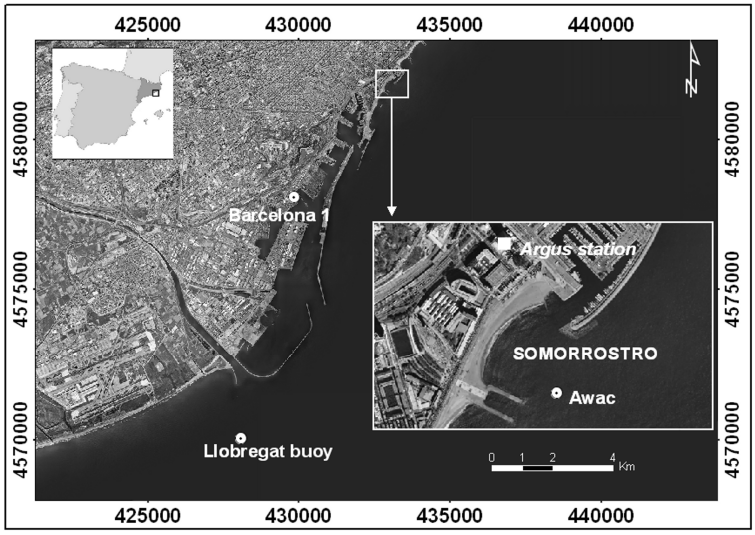

Figure 1. Study area: Argus station (square), 'Barcelona 1 tidal gauge, Llobregat deep water buoy and AWAC local wave sensor.

MATERIAL AND METHODS

The runup parameterization was evaluated using three different wave heights: 1) deep water measurements from the Llobregat buoy (www.xiom.cat, denoted here with subindex "0"); 2) local wave measurements (denoted with "1"); and 3) local wave computations propagating the Llobregat buoy conditions shorewards using the SMC (denoted with "2").

The Llobregat buoy (see Fig. 1) is located at a depth of 45 m and has provided wave height since 2001 and wave direction and peak period since 2004, recording data every hour. Three storms occurred in December 2005 and 2007 and May 2008, with maximum significant wave height above 2.5 m at the Llobregat buoy with different wave direction were selected (Table 1).

Local wave measurements were provided from a Nortek AWAC acoustic doppler current profiler (hereinafter denoted as AWAC) from the Coastal Ocean Observatory (COO, http://coo.icm.csic.es) situated at 10 m depth near the exit of the Olympic Marina (Fig. 1). The wave measurements (significant wave height, H_{s1}, and peak period, T_{p1}) were available from May 2005, although some interruptions occurred during this time. The wave direction (θ_1) was available from March 2007.

The wave transformation processes from the Llobregat buoy to Somorrostro beach were modeled for several hours of Event 3 using the SMC. The simulations presented here were carried out with the Oluca-SP package, based on spectral analysis. This model includes the effect of shoaling, refraction, energy dissipation (bottom friction and wave breaking), diffraction and wave-current interaction (Gonzalez et al., 2007). The grid had a horizontal resolution of 10 m. The wave height was recorded from SMC at the location of the AWAC (H_{s2}).

Here it is considered the astronomical and surge tides. The total tide, η, a combination of astronomical and surge tides, was obtained from the *Barcelona 1* tide gauge deployed at the Barcelona harbor (Spanish Port Authority www.puertos.es, Fig.1), recording from January 1992 to November 2008 with a few interruptions. In December 2008, this gauge was replaced and no calibrated tidal measurements were available thereafter.

Table 1. Characteristics of the storm events analyzed.

Event	Initial date	H_{s0max} (m)	T_p,H_{s0max} (s)	Θ_{mean}	Data available
1	01/12/2005	3.01	10.00	197	H_{s0}, H_{s1}
2	15/12/2007	3.5	10.00	88	H_{s0}, H_{s1}
3	08/05/2008	2.77	8.30	136	H_{s0}, H_{s1},H_{s2}

An Argus Video system (Holman and Stanley, 2007) located atop a building close to the Olympic Marina (Fig. 1) at a height of around 142 m has been deployed since 2001 (COO). The Argus station is composed of five cameras pointing at the Barcelona beaches and offering a 180º view of the coast. The

images are in the visible range of light and the sampling is done every daylight hour during a ten-minute period (1 picture per second).

The waterline position was obtained hourly from the ten-minute time-exposure (timex) images using the Intertidal Beach Mapper software (IBM, included in the Argus Runtime Environment). During the peak of the storms, some problems were often found in the waterline detection owing to the bad visibility caused by the presence of fog, clouds or rain. Hence, in these moments, and whenever there was a lack of contrast between sand and water, the waterline positions were mapped manually from the images. The image coordinates were transformed to real coordinates following the usual procedures (Holland et al., 1997). Because the images are time-averaged images, the obtained waterline position should have captured the effects of sea level (surge and astronomical tides), setup and the mean position of the fluctuations associated with the swash.

The inundation is defined here as the horizontal distance between the waterline position and the initial reference shoreline (IRS) for each event. Each IRS corresponds to a few days before the storm event, when the wave height was less than 0.5 m and the water level was approximately zero. The temporal evolution of the inundation at Somorrostro was measured following 122 profiles along the beach every 2 m; six of them, "the control profiles" (CP, profiles 10, 40, 60, 80, 100 and 122) are shown in Figure 2. The profile direction at each point was defined as perpendicular to a reference shoreline (the average of the overall IRS).

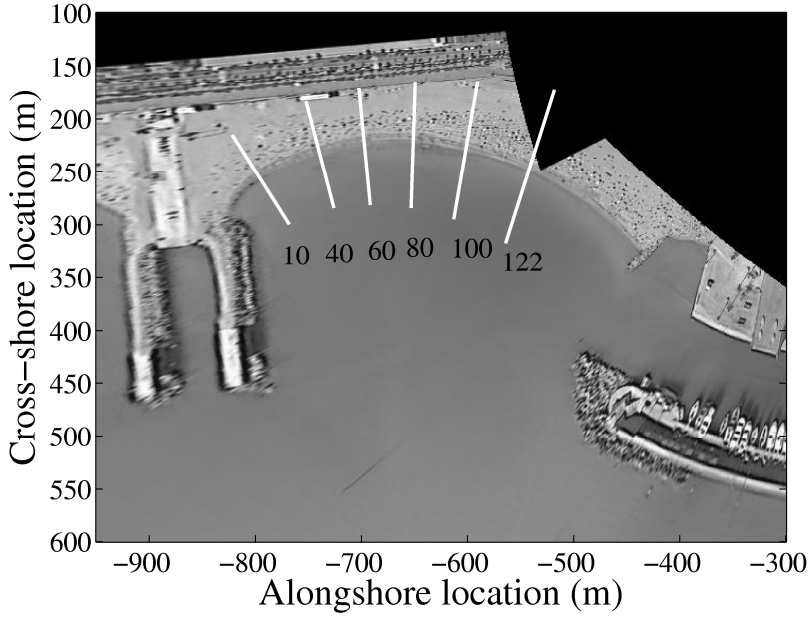

Figure 2. Argus plan view with the locations and the numbering of the control profiles.

Out of the different runup equations in the literature, the formulation by Stockdon et al. 2006 is used here because it was proposed to consider runup observations from beaches with different morphological states. This formulation, which represents the elevation of extreme runup peaks given by the 2% exceedance value, considers deep water conditions and reads:

$$R_{2\%} = 1.10\left(H_{s0} \cdot L_{p0}\right)^{0.5}\left(0.35\beta_f + \frac{\left(0.563\beta_f{}^2 + 0.004\right)^{0.5}}{2}\right) \quad (1)$$

where H_{s0} is the deep water wave height and L_{p0} the wavelength corresponding to the peak period (T_{p0}). In deep waters the dispersion relationship is:

$$L_{p0} = \frac{gT_{p0}{}^2}{2\pi}, \quad (2)$$

where g = 9.8 (m/s^2) is the gravity. In Equation (1), β_f is the foreshore beach slope. Following Ruessink et al. (1998), the foreshore slope was defined in a region between the maximum and minimum cross-shore location which can reach the runup (maximum and minimum inundation observed). Sixteen topographic d-GPS surveys were available from 2004 during calm conditions (wave height of less than 0.5 m). An average foreshore slope was calculated for each beach profile using all the available topographic data.

At beaches such as the one under consideration, the influence of the coastal structures on the wave propagation process is essential. For this reason, the runup was also computed with the above expression but using, instead of deep water conditions (H_{s0} and L_{p0}), the conditions measured with the AWAC (H_{s1} and L_{p1}) and those computed by propagating deep water conditions to the AWAC position (H_{s2} and L_{p2}). Above, the values of L_{p1} and L_{p2} are computed by iteratively solving the dispersion relationship.

The inundation observed at Somorrostro is due to the sum of the wave runup (R), astronomical tide (η_{tide}) and surge tide (η_{surge}). The observed inundation (IO) was compared with the computed inundation (IC):

$$IC = \frac{R + \eta_{tide} + \eta_{surge}}{\beta_f}, \tag{3}$$

where the runup R was parameterized as described in the above paragraphs.

The difference in the inundation is defined as Δ = IC - IO, where IC is the inundation computed using Equation (3) and IO is the observed inundation. For the *i*-th profile, the mean difference considering the observation for the *j*-th storm will be denoted here as $\Delta_{i,j}$. In addition to the difference Δ, an averaged observed inundation ($IO_{i,j}$) is used similarly.

Finally, it should be pointed out that Stockdon's formulation corresponds to the 2% runup exceedance and must therefore overpredict our observed inundation because we are using time-averaged images (timex) to measure a mean beach inundation (*i.e.* mean wave runup). However, the aim of this study is to evaluate the variability associated with the wave processes, so we used Stockdon's formulation, which takes into account beaches with different morphological states, even though the observations correspond to the 2% runup exceedance.

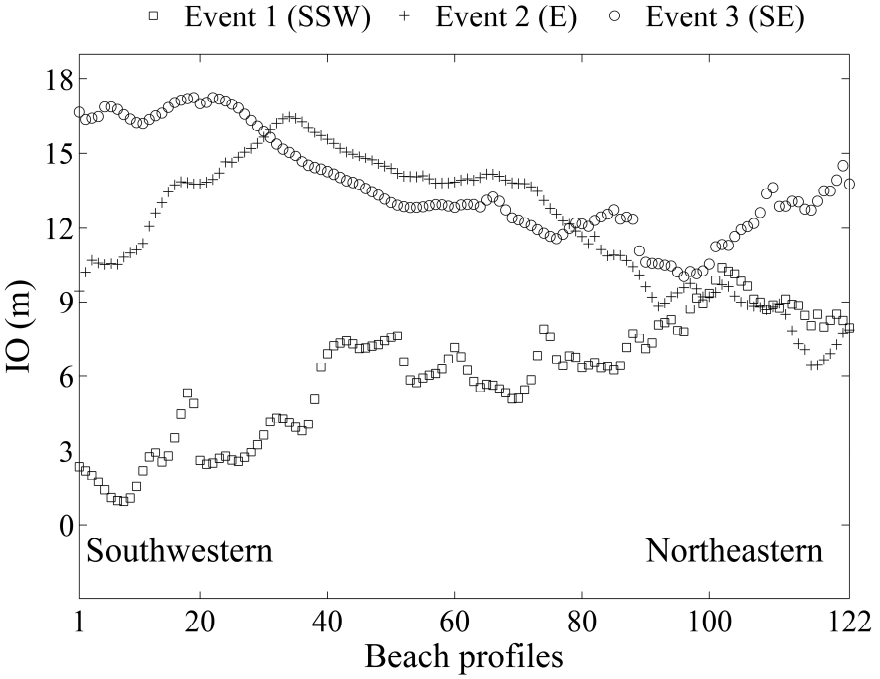

Figure 3. Alongshore distribution of the observed inundation for the maximum deep water wave height, H_{s0}, of each storm event.

RESULTS

The alongshore distribution of the inundation at Somorrostro followed a non-uniform pattern (Fig. 3). As a general trend, the northeastern area was less inundated because it is more protected from the most frequent and energetic storms (E) and also because the beach slope is higher in that part of the beach. This general pattern changed, for example, for Event 1 (SSW), in which the northeastern area was more inundated than the southwestern area (the maximum inundation values for this storm, 12 m, were found in the northeastern area) because the southwestern area is the one most protected from storms, with SSW direction.

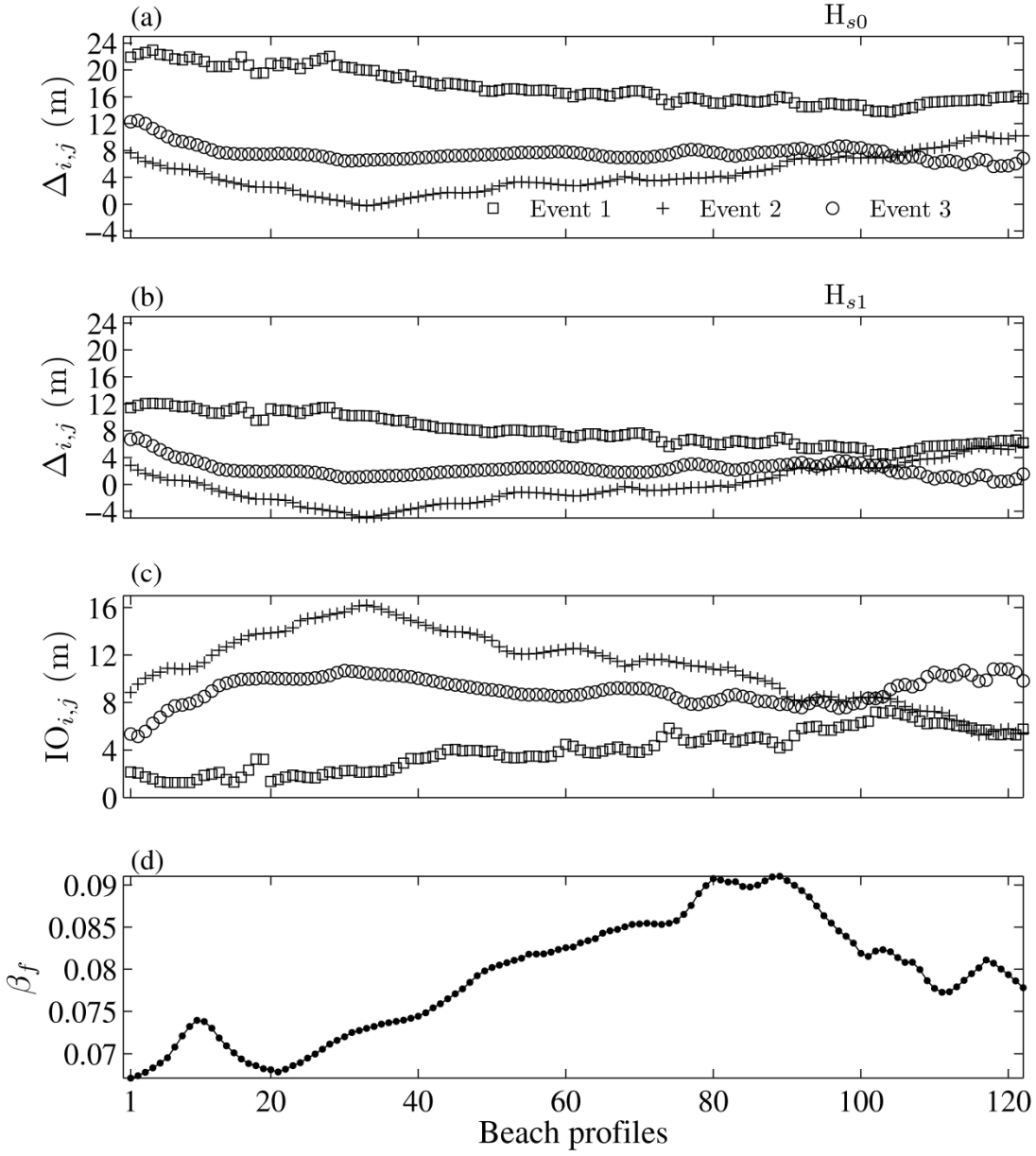

Figure 4. (a) Mean differences, $\Delta_{i,j}$, for the formulation of Stockdon et al. (2006) using Hs_0 at each storm event; (b) Mean differences, $\Delta_{i,j}$, for the formulation of Stockdon et al. (2006) using Hs_1 at each storm event; (c) Average inundation observed, $IO_{i,j}$ at each storm event for each beach profile; (d) Foreshore beach slope (β_f), for each beach profile.

The distribution of the alongshore differences, $\Delta_{i,j}$, at each storm event for all the profiles, is shown in Figure 4a using Stockdon's formulation with the deep water conditions (*i.e.*, H_{s0} and L_{p0}). As expected, this approach overestimates the inundation for all Somorrostro beach profiles on average. The

differences are not uniform alongshore: the maximum for the forth profile and at the Event 1 (SSW), where the mean inundation was $IO_{4,1}$ = 1.55 (m) (Fig. 4c), was $\Delta_{4,1}$= 22.9 m. The minimum difference was at the Event 2 (E) in the 35rd profile (Δ = 0.08 m), where the mean inundation was ($IO_{35,2}$ = 15.85 m) The central beach profiles exhibited uniform differences. Analyzing by events, the general trend, as shown in Figure 5a, was for the southwestern Event 1 to show greater differences, whereas southeastern and eastern Events 2 and 3 showed smaller differences (though still overestimating the inundation). For the sake of clarity, Figure 5 only displays the results for the six control profiles.

The difference between the observed and the computed inundation dropped when H_{s0} and L_{p0} were replaced by the local wave height measurements from the AWAC (H_{s1} and L_{p1}) in the runup expression (1), although the inundation was still overestimated (Fig. 4b). From Figure 4b, the drop in the differences between the observations and the computations when H_{s1} was used proved to be particularly important for the Event 1 (see Fig. 5b), which showed the greatest differences for deep water conditions (Fig. 5a). Thus, the differences decreased by between 8 and 10 m for Event 1 (SSW), and by around 4 m for Event 3 (SE), while the mean differences decreased by only 2 to 3 m for the eastern Event 2 (E).

Whenever direct measurements of the local wave height (H_{s1}) are unavailable, the use of a modeled local wave height (H_{s2}) has proven to give good results. In our case the correlation of H_{s1} and H_{s2} has r-squared = 0.97 and RMSE = 0.05 m. The results computed using Stockdon's formulation with H_{s1} or H_{s2} for Event 3 (this is the only event for which both H_{s1} and H_{s2} are available) were consequently similar: the differences ranged from 0.4 to 6.7 m for H_{s1} and from -0.37 to 5.3 for H_{s2}.

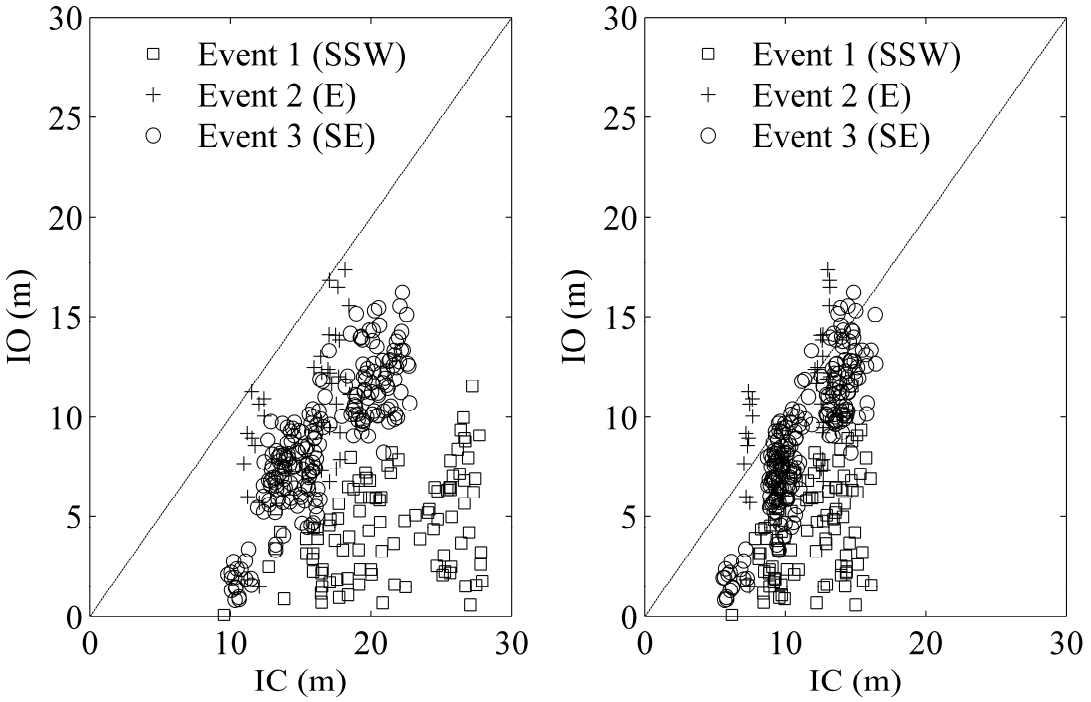

Figure 5. Observed (IO) and computed (IC) inundations in the six control profiles. (a) Using deep water conditions, H_{s0}; (b) using local conditions (10 m depth), H_{s1}.

DISCUSSION

A new engineering approach for stabilizing eroding coastlines used in the last few decades consists in creating headland-bay beaches in combination with artificial nourishments (Hsu and Evans, 1989, Klein et al., 2003). Since wave runup motions deliver much of the energy responsible for beach erosion (Sallenger, 2000; Ruggiero et al., 2001) and define the area that can be flooded, their predictability has become increasingly important for effective design of artificial embayed beaches.

Owing to the wave processes (*i.e.,* refraction and frictional dissipation across the shelf mainly), (Stockdon et al., 2006) suggested that the runup prediction using deep water buoy measurements may result in significantly higher results than those obtained using a wave height measured at a local (closer to the shore) buoy. Our results using H_{s1} (wave height measurements at 10 m depth) confirm the above statement. The differences between the inundation predicted using H_{s1} and the observations were

smaller, but the inundation was still overpredicted. Most important, this is particularly so for the southwestern Event 1 (Fig. 5), in which refraction and diffraction effects are important, and the effects on the computed inundations are clearly shown in Fig. 5.

From Fig. 6, it is clearly shown that for the southwestern Event 1, H_{s0} is almost twice higher than H_{s1}, while for the Events 2 (E) and 3 (SE) this difference is lower. Therefore, the southwestern direction of the Event 1 is where the differences between H_{s0} and H_{s1} are greatest and, consequently, in which the use of H_{s0} in Stockdon's formulation must gives the highest differences. This direction is one of the wave directions which approach Somorrostro most obliquely.

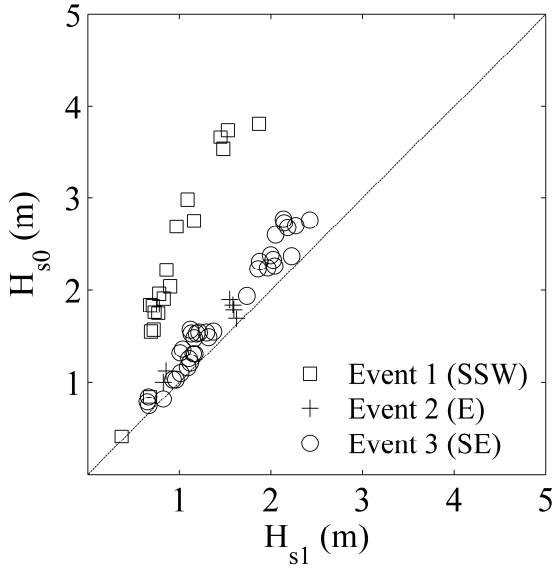

Figure 6. Comparison of H_{s0} and H_{s1} for the storms analyzed.

Embayed beaches have an asymmetric planform characterized by a strongly curved zone (in our case for the profiles (i = 1…20), a gently curved center (i = 21…80) and a relative straight section (i = 80…122). Diffraction and the refraction patterns associated with the prevailing waves determine the beach planform shape (Short and Masselink, 1999). The inundation at an embayed beach is thus linked to the beach planform shape. In our case, we usually found the greatest differences between the estimations and the observations at the southwestern end of Somorrostro, which is in the curved zone shadowed by the double dike, and also at the very northeastern end, which is affected by the Olympic Marina (Figure 4). The foreshore slope, which is related to the planform, is already taken into account in Expressions (1) and (3). The fact that the inundation differences are related to the planform suggests that the foreshore slope is not sufficient to characterize the inundation, *i.e.* that the influence of the planform (which is also affected by the wave direction) goes beyond the foreshore slope.

CONCLUSIONS

Inundation computations at a tideless embayed beach using different wave heights (H_{s0}, H_{s1}, H_{s2}) have been compared with observations. In general, the inundations computed using Stockdon's formulation with deep water conditions are higher than the observed ones (between 8 and 12 m). The difference between the computed inundation and the observations when the deep water wave height is replaced by a local wave height, H_{s1}, in the formulation of Stockdon et al., 2006 is approximately 5 m.

For engineering purposes, to define the flooded area at an embayed beach, the use of Stockdon's formulation with deep water wave measurements seems suitable since it gives results on the safe side irrespective of the wave direction. However, this formulation can give considerable differences for waves approaching obliquely to the shore and better results (still on the safe side) can be obtained using a local wave height that will take into account, to some extent, the influence of wave propagation processes on the inundation. Moreover, in the case of unavailable local wave measurements, the use of a modeled wave height, H_{s2}, is suitable. The SMC model has been shown to suitably reproduce the

wave transformation processes from deep to local water depths for a problem in which diffraction and refraction effects are great.

The distribution of the differences is heterogeneous along the beach, but follows the beach planform shape, being higher in the most curved zone, where the diffraction processes are greater. The foreshore slope is related to the beach planform shape (which is affected by the wave direction), but is not sufficient to characterize the inundation throughout the runup. Therefore, the alongshore variability of the inundation cannot be captured using either H_{s0} or H_{s1}.

ACKNOWLEDGMENTS

This study was funded by the Spanish Ministry of Science and Innovation within the IMNOBE project (CTM2009-11892). The work of the first author was supported by a JAE-predoc grant from the CSIC and co-funded by the European Social Fund (ESF). Gonzalo Simarro is supported by the Spanish government through the Ramón y Cajal program. The images used belong to the Coastal Ocean Observatory (http://coo.icm.csic.es). The authors also wish to thank the Meteorological and Oceanographic Instrument Network (XIOM) for providing the wave data of the Llobregat buoy, the Spanish Port Authority for the tide measurements and the Institute of Cartography of Catalonia (ICC) for the orthophotos used in the map of the study area.

REFERENCES

Bosom, E., Jimenez, J. A., 2011. Probabilistic coastal vulnerability assessment to storms at regional scale- application to Catalan beaches (NW Mediterranean). *Natural Hazards and Earth System Sciences*, 11 (2), 475-484.

Ciavola, P., Ferreira, O., Haerens, P., Van Koningsveld, M., Armaroli, C., Lequeux, Q., 2011. Storm impacts along European coastlines. part 1: The joint effort of the Micore and ConHaz projects. *Environmental Science & Policy*, 14 (7), 912-923.

del Rio, L., Plomaritis, T., Benavente, J., Valladares, M., P, R., 2012. Establishing storm thresholds for the Spanish Gulf of Cadiz coast. *Geomorphology*, 143-144, 13-23.

Gonzalez, M., Medina, R., Gonzalez-Ondina, J., Osorio, A., Mendez, F. J., Garcia, E., 2007. An integrated coastal modeling system for analyzing beach processes and beach restoration projects, SMC. *Computers & Geosciences*, 33 (7), 916-931.

Guza, R. T., Thornton, E. B., 1982. Swash oscillations on a natural beach. *Journal of Geophysical Research-Oceans and Atmospheres*, 87 (NC1), 483-491.

Holland, K. T., Holman, R. A., Lippmann, T. C., Stanley, J., Plant, N., 1997. 480 Practical use of video imagery in nearshore oceanographic field studies. *IEEE Journal of Oceanic Engineering*, 22 (1), 81-92.

Holman, R., Stanley, J., 2007. The history and technical capabilities of Argus. *Coastal Engineering*, 54, 477-491.

Hsu, J. R. C., Evans, C., 1989. Parabolic bay shapes and applications. *Proceedings of the Institution of Civil Engineers Part 2-research and Theory*, 87, 557-570.

Klein, A. H. D., Vargas, A., Raabe, A. L. A., Hsu, J. R. C., 2003. Visual assessment of bayed beach stability with computer software. *Computers & Geosciences*, 29 (10), 1249-1257.

Ojeda, E. and Guillén, J.,2008. Shoreline dynamics and beach rotation of artificial embayed beaches. *Marine Geology*, 253, 51–62.

Ruessink, B., Kleimhans, M., van del Beukel P.G.L., 1998. Observations of swash under highly dissipative conditions. *Journal of Geophysical Research*, 12 103 (2), 3111-3118.

Ruggiero, P., Komar, P., McDougal, W. G., M., J.J., Beach, R., 2001. Wave runup, extreme water levels and the erosion of properties backing beaches. *Journal of Coastal Research*, 17 (2), 407-419.

Sallenger, A. H., 2000. Storm impact scale for barrier islands. *Journal of Coastal Research*, 16 (3), 890-895.

Short, A., Masselink, G., 1999. *Handbook of Beach and Shoreface Morphodynamics*. Willey, Ch. Embayed and structurally controlled beaches, pp. 230-249.

Stockdon, H., Holman, R.A., Howd, P.A., and Sallenger Jr., A.H. 2006. Empirical parameterization of setup, swash and runup. *Coastal Engineering*, 53, 573-588.

Wolf, J., 2009. Coastal flooding: impacts of coupled wave-surge-tide models. *Natural Hazards*, 49 (2), 241-260